

bradscholars

Bond behaviors between nano-engineered concrete and steel bars

Item Type	Article
Authors	Wang, X.;Dong, S.;Ashour, Ashraf;Ding, S.;Han, B.
Citation	Wang X, Dong S, Ashour A et al (2021) Bond behaviors between nano-engineered concrete and steel bars. Construction and Building Materials. 299: 124261.
DOI	https://doi.org/10.1016/j.conbuildmat.2021.124261
Publisher	Elsevier
Rights	© 2021 Elsevier Ltd. All rights reserved. Reproduced in accordance with the publisher's self-archiving policy. This manuscript version is made available under the Creative Commons CC-BY-NC-ND license (https://creativecommons.org/licenses/by-nc-nd/4.0/)
Download date	2026-06-08 17:15:49
Link to Item	http://hdl.handle.net/10454/18564

Bond behaviors between nano-engineered concrete and steel bars

Xinyue Wang¹, Sufen Dong^{2,*}, Ashraf Ashour³, Siqi Ding⁴, Baoguo Han^{1,*}

¹*School of Civil Engineering, Dalian University of Technology, Dalian, 116024 China*

²*School of Transportation and Logistics, Dalian University of Technology, Dalian 116024, China*

³*Faculty of Engineering & Informatics, University of Bradford, Bradford, BD7 1DP, UK*

⁴*Department of Civil and Environmental Engineering, The Hong Kong Polytechnic University, Hung Hom, Kowloon, Hong Kong*

* Corresponding author: hithanbaoguo@163.com, dongsufen@dlut.edu.cn

Abstract:

This paper investigated the bond characteristics between eight types of nanofillers modified reactive powder concrete (RPC) and plain steel bars, aiming to explore the modifying mechanisms and establish a bond-slip relationship model for nanofillers modified RPC and steel bar interface. The experimental results indicated that the incorporation of nanofillers can increase the bond strength and reduce the slip between RPC and plain steel bars. It was shown that a 2.15 MPa/20.5% of absolute/relative increase in cracking bond strength, a 1.25 MPa/10.3% of absolute/relative increase in ultimate bond strength, a 2.35 MPa/22.4% of absolute/relative increase in residual bond strength, a 0.592 mm/56.5% of absolute/relative reduction in ultimate bond slip, and a 1.779 mm/52.1% of absolute/relative reduction in residual bond slip were the best achieved due to the addition of various nanofillers. The enhancement of nanofillers on RPC-steel bar interface has been mainly attributed to RPC microstructure improvement, optimization of intrinsic compositions, and elimination of defects in the interface, especially the underside near steel bar, due to the nano-core effect of nanofillers enriched in the interface. In addition, the bond-slip relationship of nanofillers modified RPC-steel bar interface can be accurately described by the proposed model considering an initial branch.

Keywords: Nano-engineered concrete-steel bar interface; Nanofillers; Bond characteristics; Modifying mechanisms; Bond-slip model

30 1 Introduction

31 As one of the most widely used construction materials in civil engineering, reinforced
32 concrete possesses superior mechanical performance and durability due to the
33 combination of high compressive strength and good erosion resistance of concrete and
34 excellent tensile performance of reinforcing bars [1–3]. However, a key parameter in
35 achieving the composite action is the bond characteristics between concrete and
36 reinforcing bars. A reliable bond ensures stress transfer and corrosion inhibition in
37 reinforced concrete, leading to good serviceability of reinforced concrete structures [4,
38 5]. Bond strength is generally developed by chemical-physical adhesion, mechanical
39 micro-interlocking, and friction between concrete and reinforcing bars, which is mainly
40 influenced by the reinforcing bar characteristics (such as physical dimension [6],
41 chemical composition [7], and surface roughness [8]), concrete performance (such as
42 mechanical properties [9] and shrinkage [10]), anchorage length [11], and loading state
43 [12]. Considering the fact that concrete-reinforcing bar debonding is essentially
44 concrete failure in the interfacial zone, enhancing concrete performance can
45 fundamentally modify the bond characteristics between concrete and reinforcing bar,
46 and consequently, improve the performance of reinforced concrete.

47 Reactive powder concrete (RPC), as an innovative type of concrete with ultra-high
48 performance, possesses superior strength, good durability, and excellent volume
49 stability [13–15]. Owing to these excellent merits, bond between RPC and reinforcing
50 bars is significantly higher compared with that between ordinary concrete and
51 reinforcing bars [16–18]. Previous studies have demonstrated that the bond strength of
52 RPC-reinforcing bar interface is approximately 6–28% higher than that of ordinary
53 concrete-reinforcing bar interface [19–21] and the bond stiffness between concrete and
54 reinforcing bars can also increase [22, 23]. Although RPC has great potential

55 application in reinforced concrete elements or structures, many researches have been
56 dedicated to further optimize this promising concrete material. Nanotechnology, as a
57 leading industry in the 21st century, provides new opportunities to further improve the
58 performance of RPC as nanofillers can tailor the structures of concrete materials at
59 nanoscale, affecting the structures and performance of concrete [24-26]. For example,
60 compared with RPC without nanofillers, adding nano-TiO₂, carbon nanotubes (CNTs),
61 and multi-layer graphene can absolutely/relatively increase the compressive strength
62 by 12.2 MPa/12.3%, 18.5 MPa/18.1%, and 22.1 MPa/21.9%, as well as the flexural
63 strength by 6.69 MPa/87%, 3.84 MPa/27.2%, and 2.0 MPa/20.7%, respectively [27–
64 29]. Additionally, nanofillers have the unique enrichment effect on the interfacial zone
65 in RPC, which can significantly improve the interfacial bonding behavior [30].
66 Therefore, it is conceived that the nanofillers and RPC may exert astonishing
67 synergistic effects on bond between concrete and reinforcing bars, aiming at improving
68 the bearing capacity, stiffness, and service life of reinforced concrete elements and
69 structures. However, there are little studies on the bond characteristics between
70 nanofillers modified RPC and reinforcing bars. Meanwhile, the deep understanding of
71 modifying mechanisms and the appropriate model for describing the nanofiller
72 modified RPC-reinforcing bar bond characteristics are urgently required in order to
73 control and design the interface between nanofillers modified RPC and reinforcing bars.

74 Herein, this paper aims to investigate the bond characteristics between nanofillers
75 modified RPC and reinforcing bars. For this purpose, a pull-out test was performed to
76 characterize the bond between eight types of nanofillers modified RPC and reinforcing
77 bars. After the pull-out test, scanning electron microscope (SEM) and energy dispersive
78 x-ray spectrometry (EDX) were carried out to examine the interfacial microstructures,
79 chemical composition, and nanofiller distribution. Finally, a bond-slip model was

80 proposed for nanofiller modified RPC and reinforcing bars based on the experimental
 81 results.

82 2 Experimental schemes

83 2.1 Raw materials and mix proportions

84 The binders used in RPC included ordinary Portland cement with a strength grade of
 85 42.5 R, class II fly ash, and silica fume with a particle size between 0.05–0.15 μm . The
 86 fine aggregates were quartz sand with a particle size ranging from 0.12 mm to 0.83 mm.
 87 The polycarboxylate superplasticizer with a 30% reducing water capability was used as
 88 a water reducer. In this study, the selected nanofillers included 0-D (nano-SiO₂, nano-
 89 TiO₂, nano-ZrO₂), 1-D (CNTs, hydroxyl functionalized CNTs (H-CNTs), nickel-coated
 90 CNTs (Ni@CNTs)), and 2-D (multi-layer graphene, and nano-BN) nanofillers, and
 91 their properties are listed in Table 1. According to references [31, 32], steel bars are
 92 currently the most used reinforcement in concrete structures, and bond between
 93 concrete and plain steel bars is of fundamental significance for the assessment of the
 94 overall structural behavior of reinforced elements or structures. Therefore, the hot-
 95 rolled plain steel bar with a diameter of 6.5 mm, a yield strength of 300 MPa, and an
 96 ultimate strength of 420 MPa was selected as the reinforcing bar in this study. In
 97 addition, all steel bars were polished with sandpaper to ensure similar surface roughness.

98
 99

Table 1. Properties of nanofillers

Types	Purity (%)	Diameter (nm)	Length (μm)	Thickness (nm)	Specific surface area (m^2/g)
Nano-SiO ₂	≥ 99	20	–	–	≥ 600
Nano-TiO ₂	≥ 96	20	–	–	–
Nano-ZrO ₂	≥ 99	20	–	–	≥ 25
CNTs	–	20–30	0.5–2	–	> 120
Hydroxyl functionalized CNTs	–	< 8	0.5–2	–	> 380
Nickel-coated CNTs	–	20–30	10–30	–	70
Multi-layer graphene	–	< 2000	–	1–5	500
Nano BN	99.9	120	–	5–100	19

100

101 To achieve good mechanical performance of RPC, the raw materials and mix
 102 proportions of RPC without and with nanofillers were determined according to the
 103 former studies [30], as illustrated in Table 2. It is worth noting that the dosage of water
 104 reducer was adjusted to achieve similar workability of RPC with different types and
 105 contents of nanofillers.

106
 107

Table 2. Mix proportions of RPC without and with nanofillers

Specimen code	Nanofillers	Mix proportions (kg/m ³)						
		Cement	Nanofillers	Fly ash	Silica fume	Fine aggregate	Water	Water reducer
Control	–	750	–	187.5	234.7	1031.2	281.2	11.3
S-1		742.5	7.5					15.0
S-2	Nano-SiO ₂	735.0	15.0	187.5	234.7	1031.2	281.2	18.8
S-3		727.5	22.5					22.5
T-1		742.5	7.5					
T-2	Nano-TiO ₂	735.0	15.0	187.5	234.7	1031.2	281.2	11.3
T-3		727.5	22.5					
Z-1		742.5	7.5					
Z-2	Nano-ZrO ₂	735.0	15.0	187.5	234.7	1031.2	281.2	11.3
Z-3		727.5	22.5					
C-0.1		749.2	0.8					
C-0.3	CNTs	747.7	2.3	187.5	234.7	1031.2	281.2	11.3
C-0.5		746.2	3.8					
H-0.1		749.2	0.8					
H-0.3	H-CNTs	747.7	2.3	187.5	234.7	1031.2	281.2	11.3
H-0.5		746.2	3.8					
N-0.1		749.2	0.8					
N-0.3	Ni@CNTs	747.7	2.3	187.5	234.7	1031.2	281.2	11.3
N-0.5		746.2	3.8					
M-0.1		749.2	0.8					
M-0.3	Multi-layer graphene	747.7	2.3	187.5	234.7	1031.2	281.2	11.3
M-0.5		746.2	3.8					
B-0.1		749.2	0.8					
B-0.3	Nano-BN	747.7	2.3	187.5	234.7	1031.2	281.2	11.3
B-0.5		746.2	3.8					

108

109 2.2 Specimen preparation

110 In this study, specimens for the pull-out test were fabricated, and the geometrical
 111 dimensions of the specimens is shown in Figure 1 (a). The detailed process of specimen
 112 preparation is illustrated in Figure 2. It is noteworthy that this study used
 113 polycarboxylate superplasticizer as dispersing agent. Additionally, stirring and
 114 ultrasonic were applied for dispersing non-carbon nanofillers (namely Nano-SiO₂,

115 Nano-TiO₂, Nano-ZrO₂, and nano BN) and carbon nanofillers (namely CNTs, Hydroxyl
 116 functionalized CNTs, Nickel-coated CNTs, and multi-layer graphene), respectively.
 117 The aforementioned methods can ensure the uniform distribution of nanofillers in RPC
 118 according to previous investigations [26].
 119

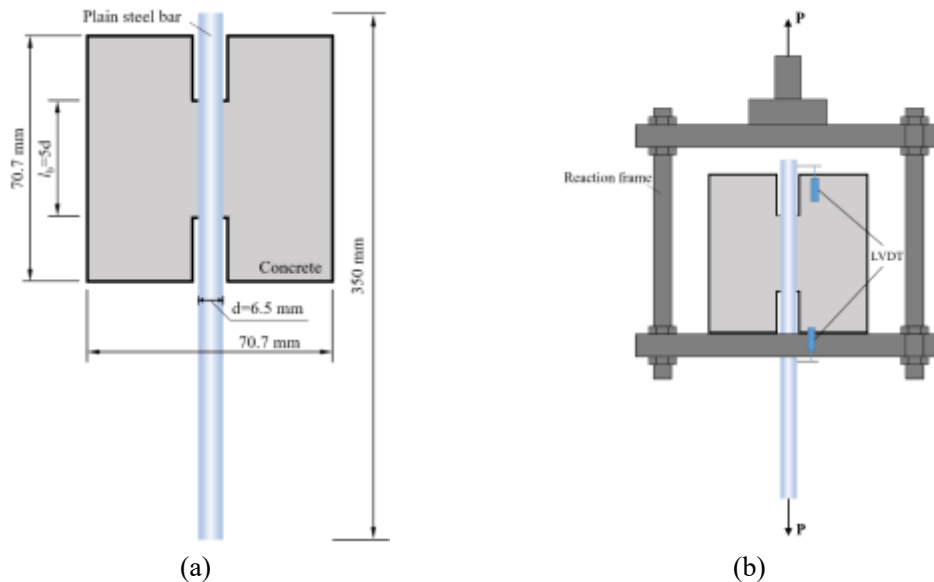


Figure 1. Schematic diagrams of (a) Specimen dimensions; (b) The pull-out test

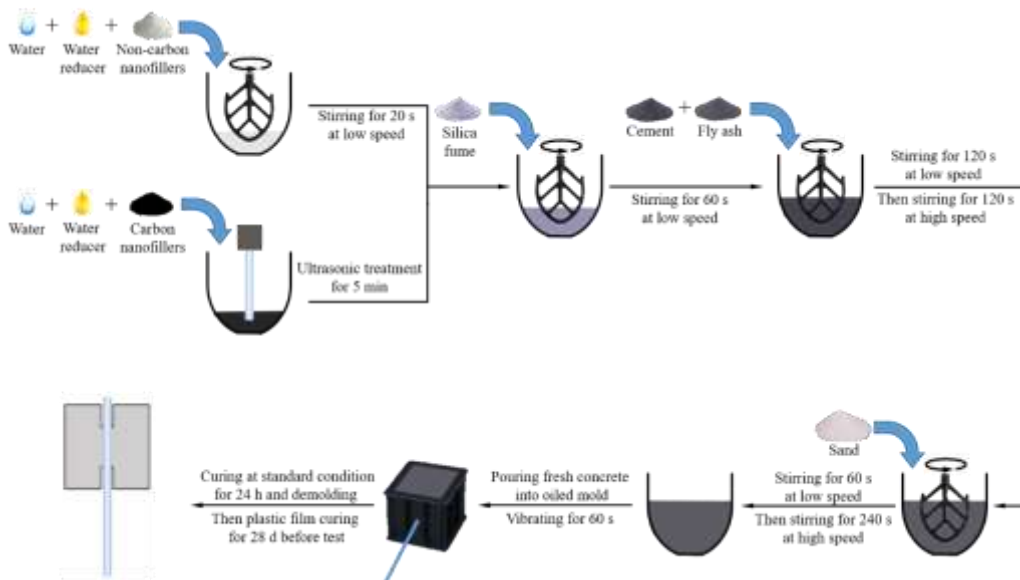


Figure 2. The process of specimen preparation

120

121 2.3 Measurements

122 The pull-out test was performed to characterize the nanofiller modified RPC-steel
 123 bar bond characteristics, as shown in Figure 1 (b). According to reference [33], the steel

124 bars were pulled out of the RPC cube at a constant loading rate of 0.5 mm/min. The
125 average bond stress τ_b between RPC and steel bar can be calculated from Equation
126 (1).

$$\tau_b = \frac{P}{\pi d l_b} \quad (1)$$

127 where P is the pull-out load, d is the diameter of steel bar, and l_b is the bonded
128 length. In addition, the slips at the loading end and free end of the steel bar were
129 measured by two LVDTs (linear variable differential transformers). The average slip s
130 of the steel bar can be calculated from Equation (2).

$$s = (s_l + s_f)/2 \quad (2)$$

131 where s_l and s_f are the slips at the loading end and free end of the steel bar,
132 respectively. The bond stress-slip curve was determined based on the experimental
133 results of τ_b and s , and the bond strength of each group equaled to the average of the
134 bond strengths of three specimens.

135 Considering that the steel bars are placed horizontally during casting, the
136 microstructures of the interface between RPC and the upside and underside (during
137 casting) of steel bars could be different due to the internal water bleeding [34].
138 Therefore, SEM was performed on the failure surfaces of RPC bonding, both the upside
139 and underside (during casting) surfaces of steel bars, respectively. Afterward, the
140 chemical compositions of the hydration products in the interface of specimens
141 without/with nanofillers were identified by EDX. Additionally, EDX mapping analysis
142 was performed to characterize the distribution of nanofillers. According to reference
143 [35, 36], the number and brightness of the points of EDX mapping image can represent
144 the content of target element, which can be used for reflecting the local content of
145 nanofillers in the analysis area. Therefore, the EDX mapping images are firstly
146 converted into gray-scale images, and the average gray value is calculated [37]. In this

147 way, the average gray value of the EDX mapping image can indicate the local content
148 of nanofillers in the analysis area. Noteworthily, EDX mapping analysis can only
149 characterize the distribution of nanofillers that have different elements from the
150 components of RPC and the elements introduced in sample pretreatment. Therefore,
151 EDX mapping analysis was only performed on the specimens with nano-TiO₂, nano-
152 ZrO₂, and nano-BN.

153 3 Results and Discussions

154 3.1 Bond characteristics

155 In this experiment, all specimens showed pull-out failure, namely, the steel bars were
156 pulled out of RPC cubes rather than RPC splitting or steel bar fracture. Figure 3 shows
157 the typical bond stress-slip curve and the schematic diagram of composition of bond
158 stress in different branches. On the basis of failure state, the cracking bond strength
159 $\tau_{b,0}$, ultimate bond strength $\tau_{b,u}$, and residual bond strength $\tau_{b,r}$ and the
160 corresponding slips were selected as characteristic parameters of bond stress-slip curves,
161 as listed in Table 3. According to these strengths and slips, the bond stress-slip curve
162 can be divided into four branches: initial, ascending, descending, and residual branches.

163 1) Initial branch (OA)

164 In the initial branch, the bond stress between RPC and steel bars does not exceed the
165 chemical-physical adhesion (mainly van der Waals force), that is to say, the RPC-steel
166 bar interface is well bonded without cracks. Therefore, the slip between RPC and steel
167 bar is almost zero until the bond stress reaches the cracking bond strength. As shown in
168 Table 3, adding nanofillers can increase the absolute/relative cracking bond strength of
169 RPC-steel bar interface by 2.15 MPa/20.5%, 1.60 MPa/15.3%, 1.35 MPa/12.9% when
170 1 wt.% of nano-TiO₂, 0.1 wt.% of H-CNTs, and 0.5 wt.% of nano-BN were incorporated,
171 respectively.

172 It is noteworthy that the initial branch is not observed when the strength of concrete
173 is low [38–41]. Additionally, according to references [42, 43], the bond stress in
174 practical civil engineering structures is approximately 1.9–4.1 MPa, which is below the
175 cracking bond strength in this study. Therefore, the appearance of initial branch and
176 enhancement of cracking bond strength can ensure the reinforced concrete structures
177 working without cracks between RPC and steel bars. The crack-free bond, on the one
178 hand, is conducive to the stress transfer between RPC and steel bars, leading to a great
179 composite effect on the mechanical performance of reinforced concrete. On the other
180 hand, it is beneficial to hinder the invasion of harmful substances in the concrete and
181 prevent the corrosion of steel bars, prolonging the service life of reinforced concrete
182 elements and structures.

183 2) Ascending branch (AB)

184 When the bond stress exceeds the cracking bond strength between RPC and steel bar,
185 the RPC-steel bar interface near the loading end begins to crack. After the local cracks
186 occurring, the bond stress between RPC and debonded steel bars derives from the
187 micro-interlocking between RPC and steel bar with tiny irregularities on the surface
188 [44]. As the cracks gradually develop, the bond-slip curve shows a non-linear
189 relationship until the average bond stress reaches the ultimate bond strength. The
190 addition of 2 wt.% of nano-SiO₂, 0.5 wt.% of H-CNTs, 0.5 wt.% of nano-BN can
191 increase the absolute/relative ultimate bond strength by 1.25 MPa/10.3%, 0.98
192 MPa/8.1%, 1.24 MPa/10.2%, respectively. The improvement of ultimate bond strength
193 indicates the incorporation of nanofillers increases the reliability of the bond between
194 RPC and steel bars. In addition, the slip at the ultimate bond strength s_u generally
195 decreases after the addition of nanofillers. The slips are absolutely/relatively decreased
196 by 0.592 mm/56.5%, 0.522 mm/49.8%, and 0.492 mm/46.9% when 2 wt.% of nano-

197 TiO₂, 0.1 wt.% of CNTs, and 0.1 wt.% of nano-BN were incorporated, respectively. The
198 reduction of the ultimate slips is beneficial to increase the stiffness of reinforced
199 concrete structures [45].

200 3) Descending branch (BC)

201 With the increase of the slip, the debonding section of the RPC-steel bar interface
202 develops and extends from the loading end to the free end along the steel bars. The
203 micro-interlocking effect is gradually lost due to the local RPC crushing. The bond
204 stress between the RPC and steel bars is borne by the friction between them [44]. With
205 the continuous deterioration of RPC in the interfacial zone, the friction coefficient of
206 the interface between RPC and steel bar decreases. Therefore, in the descending branch,
207 the bond stress decreases gradually, and the slip amount increases greatly. The residual
208 bond strengths of composites with 2 wt.% of nano-SiO₂, 0.3 wt.% of H-CNTs, and 0.5
209 wt.% of nano-BN are absolutely/relatively increased by 1.86 MPa/17.7%, 2.35
210 MPa/22.4%, and 1.78 MPa/17.0%, respectively, compared with that of specimens
211 without nanofillers. As for the residual slip, adding 3 wt.% of nano-TiO₂, 0.3 wt.% of
212 H-CNTs, and 0.5 wt.% of multi-layer graphene can absolutely/relatively decrease the
213 residual slip by 1.525 mm/44.7%, 1.779 mm/52.1%, and 1.575 mm/46.1%, respectively.
214 These phenomena suggest the microstructure of the interface in RPC with nanofillers
215 reaches a new stable state in a shorter slip. Meanwhile, the new stable state of interface
216 in RPC with nanofillers is relatively complete, resulting in a higher residual bond
217 strength. The increase of residual bond strength can provide a certain bond strength
218 after the failure, which can improve the ductility of reinforced concrete structure, avoid
219 brittle failure, and gain time for structural monitoring, safety warning, and later
220 repairing.

221 4) Residual branch (CD)

222 In the residual branch, the state of interface in RPC is stable, and the bond stress is
 223 borne by the sliding friction between RPC and steel bar [44]. The bond stress maintains
 224 at a stable level with the pull-out distance increasing.
 225

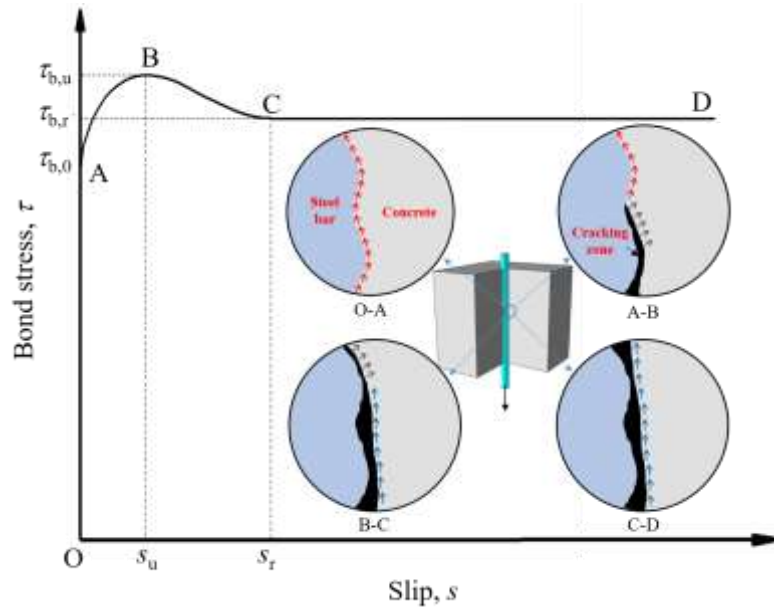


Figure 3. Typical bond stress-slip curve and the schematic diagram of the composition of bond stress at different branches (red arrows refer to the chemical-physical adhesion, grey arrows refer to the micro-interlocking, and blue arrows refer to the friction)

226 Table 3. Characteristic parameters of bond stress-slip curves of specimens without/with nanofillers

Code	$\tau_{b,0}$ (MPa)	$\tau_{b,u}$ (MPa)	s_u (mm)	$\tau_{b,r}$ (MPa)	s_r (mm)
Control	10.48	12.10	1.048	10.50	3.415
S-1	11.55	12.20	0.791	11.06	2.762
S-2	12.13	13.35	0.611	12.36	2.334
S-3	11.94	12.85	0.644	11.50	2.558
T-1	12.63	12.99	0.832	11.10	2.950
T-2	12.40	12.74	0.456	11.66	2.038
T-3	12.49	13.14	0.467	12.18	1.890
Z-1	12.06	13.16	0.994	10.88	3.695
Z-2	12.12	12.74	1.055	11.16	2.761
Z-3	11.27	12.72	0.728	10.84	2.329
C-0.1	11.88	12.95	0.526	11.10	2.602
C-0.3	10.79	12.96	0.697	11.75	2.276
C-0.5	11.04	12.84	1.126	10.96	2.79
H-0.1	12.08	12.91	0.619	11.59	1.966
H-0.3	11.34	13.01	0.600	12.85	1.636
H-0.5	11.93	13.08	0.705	11.76	1.873
N-0.1	11.21	13.07	0.979	11.34	2.697
N-0.3	10.34	12.96	0.752	11.83	3.053
N-0.5	11.51	12.96	0.774	12.21	2.490
M-0.1	11.41	12.35	0.637	11.51	2.116
M-0.3	11.68	12.62	0.561	11.98	2.066
M-0.5	9.51	12.34	0.610	11.98	1.840
B-0.1	10.91	13.04	0.556	12.05	2.098
B-0.3	11.24	13.19	0.741	10.99	2.322

227

228 3.2 Modifying mechanisms

229 The modifying mechanisms of nanofillers on the RPC-steel bar interface were
230 revealed by SEM observation and EDX analysis. As mentioned in section 2.3, the
231 average gray value of the EDX mapping image can indicate the local content of
232 nanofillers. As shown in Figure 4, the average gray values of EDX mapping images of
233 RPC with 3 wt.% of nano-TiO₂, 1 wt.% of nano-ZrO₂, and 0.5 wt.% of nano-BN are
234 7.22, 17.51, and 8.35, respectively. Meanwhile, regarding the interface between RPC
235 and the upside/underside of steel bar (during casting), the average gray values of EDX
236 mapping images of specimens with 3 wt.% of nano-TiO₂, 1 wt.% of nano-ZrO₂, and 0.5
237 wt.% of nano-BN are 16.80/10.81, 33.48/29.21, and 12.35/8.85, respectively. Therefore,
238 it can be concluded that the local content of nanofillers in the RPC-steel bar interface
239 is higher than that in nanofillers modified RPC. Additionally, the local content of
240 nanofillers in the RPC-steel bar interface near the upside of steel bar (during casting) is
241 higher than that near the underside of steel bar.

242 Based on the results of EDX mapping analysis, it can be seen that nanofillers enrich
243 in the RPC-steel bar interface. The distribution characteristic of nanofillers may be
244 attributed to the wall effect [46] and the gravity effect [47]. The wall effect suggests
245 that the zone closest to the steel bar contains smaller particles, while larger particles
246 tend to appear in the area further from the surface of steel bar during casting [46]. Due
247 to the small size of nanofillers, the wall effect leads to form a nanofiller enrichment
248 layer in the RPC-steel bar interface, as shown in Figure 5. In addition, the local content
249 of nanofillers in the RPC-steel bar interface near the upside of steel bar (during casting)
250 is higher than that near the underside of steel bar, which can be attributed to the gravity
251 effect [47]. The nanofillers tend to sink in the fresh RPC due to the higher density

252 (Figure 5), resulting in the higher local content of nanofillers in the interface between
253 RPC and the upside of steel bar.

254

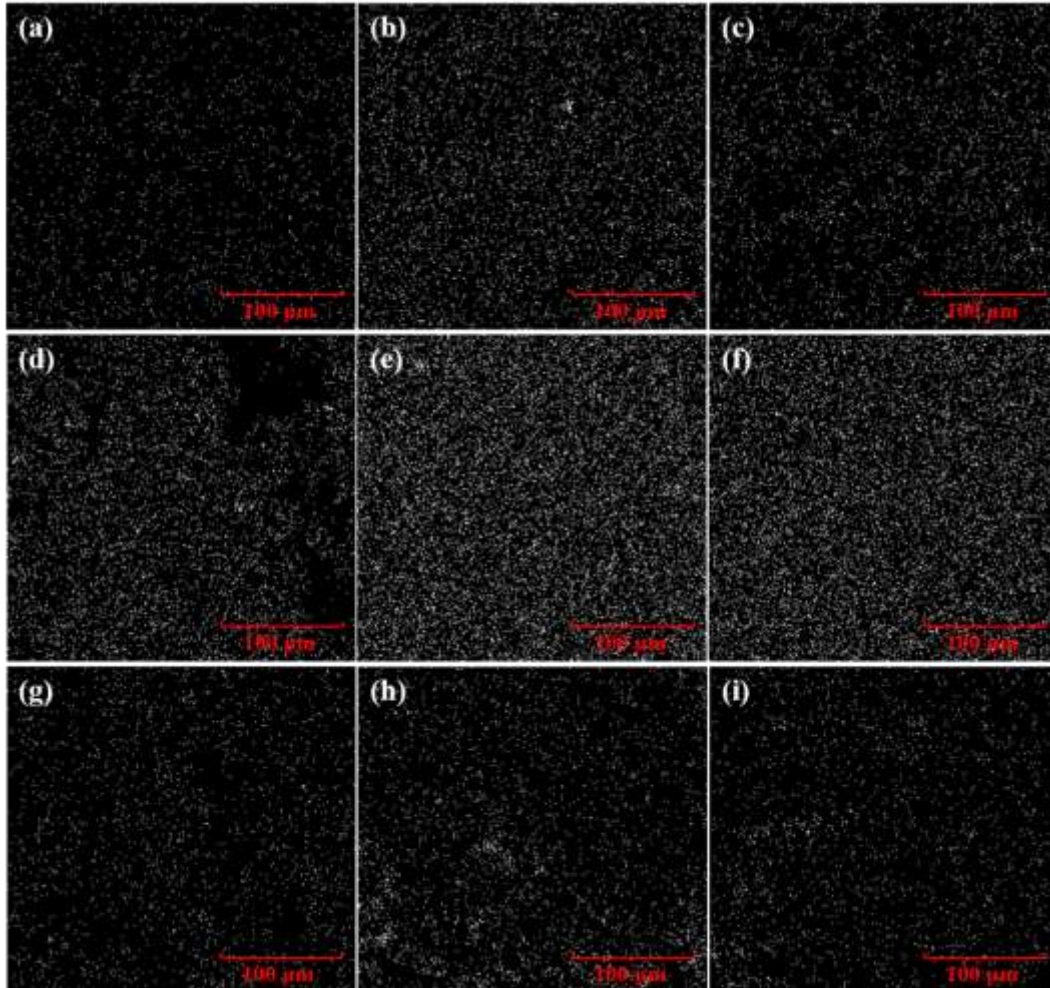


Figure 4. EDX mapping images for characterizing the distribution of (a) Titanium in RPC, (b) Titanium in the interface near the upside of steel bar, and (c) Titanium in the interface near the underside of steel bar of the specimen with 3 wt.% of nano-TiO₂; (d) Zirconium in PRC, (e) Zirconium in the interface near the upside of steel bar, and (f) Zirconium in the interface near the underside of steel bar of the specimen with 1 wt.% of nano-ZrO₂; (g) Nitrogen in RPC, (h) Nitrogen in the interface near the upside of steel bar, and (i) Nitrogen in the interface near the underside of steel bar of the specimen with 0.5 wt.% of nano-BN

255

256

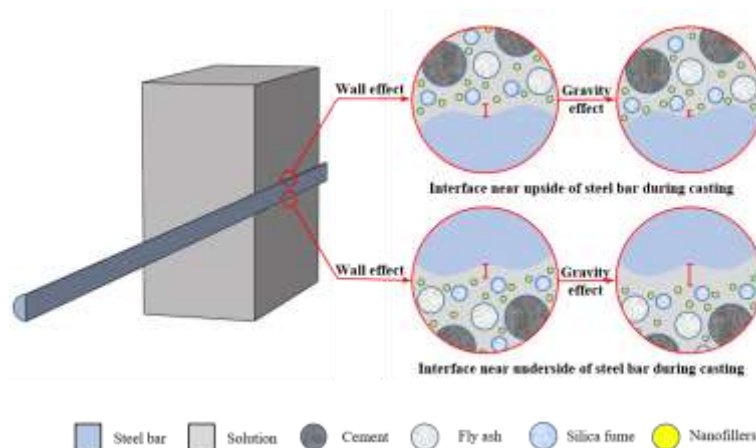


Figure 5. The formation of nanofiller enrichment in RPC-steel bar interface near the upside and underside of steel bar during casting

257

258 The microstructures of interface between RPC without/with nanofillers and steel bar

259 are illustrated in Figures 6–9. The original morphology of hydration products in the

260 interface between RPC without nanofillers and upside of steel bar is loose and porous

261 (Figure 6 (a)), while that in the interface between RPC and underside of steel bar are

262 more compact (Figure 6 (c)). Additionally, the molar ratios of CaO to SiO₂ (Ca/Si ratio)

263 of C-S-H gels on the interface near the upside and underside of steel bar are 0.86 and

264 1.02 respectively. These phenomena may attribute to the water bleeding under the steel

265 bar. The water bleeding leads to the increase of local water-to-binder ratio, resulting in

266 loose microstructures and a high Ca/Si ratio of interface near the underside of steel bar.

267 After the pull-out test, many cracks appear on the failure surface near the upside and

268 underside of steel bar (during casting). In addition, the interfacial RPC shows stripping

269 failure state, like scales, as depicted in Figure 6 (b) and (d).

270 The presence of nanofillers can notably modify the microstructure of RPC-steel bar

271 interface, as depicted in Figures 7–9. Adding nanofillers can make the original

272 morphology of hydration products more uniform and compact, especially the hydration

273 products on the interface near the underside of steel bar. In addition, the presence of

274 nanofillers leads to the decrease of Ca/Si ratio. The Ca/Si ratio of C-S-H gels on the

275 interface between RPC and upside/underside of steel bar is absolutely/relatively

276 reduced to 0.83/1.02, 0.65/0.89, and 0.75/0.92 when 3 wt.% of nano-TiO₂, 0.5 wt.% of
277 H-CNTs, and 0.5 wt.% of nano-BN are added. The improvement of hydration products
278 and the optimization of Ca/Si ratio of C-S-H gels lead to a reliable bond between
279 nanofillers modified RPC and steel bar, resulting in the improvement of cracking bond
280 strength in the pull-out test. After the pull-out test, fewer cracks appear on the surfaces
281 of failure surface of specimens with nanofillers compared to that without nanofillers,
282 additionally, the cracks show in-plane cracking. It can be concluded that the presence
283 of nanofillers increases the integrity of RPC-steel bar interface after the pull-out test,
284 which helps enhance the micro-interlocking and friction between RPC and steel bar,
285 thereby improving the ultimate bond strength and resident bond strength.

286

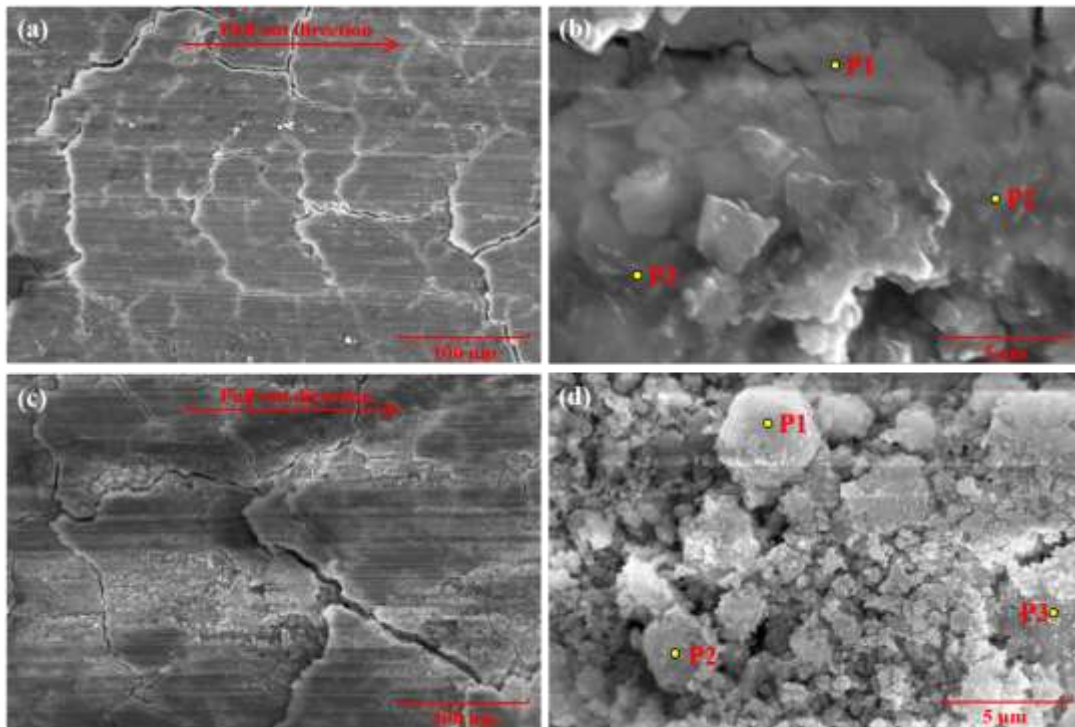


Figure 6. The microstructures of (a) and (b) Interface between plain RPC and upside of steel bar (1000×) and (20000×); (c) and (d) Interface between plain RPC and underside of steel bar (1000×) and (20000×)

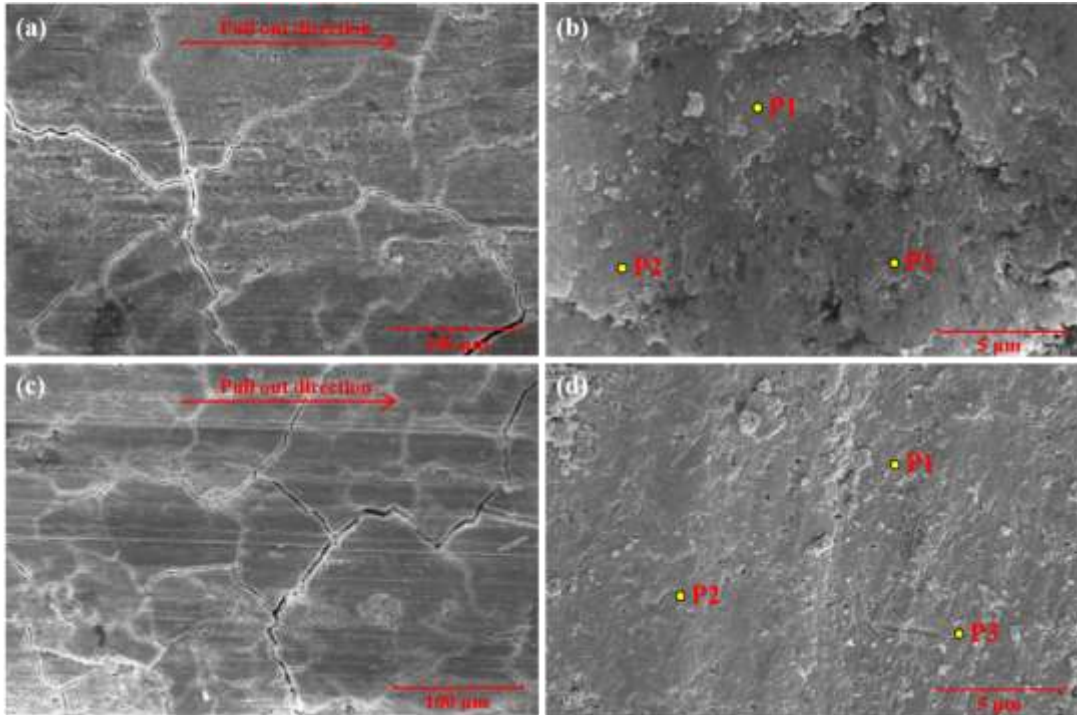


Figure 7. The microstructures of (a) and (b) Interface between RPC with 3 wt.% of nano-TiO₂ and upside of steel bar (1000×) and (20000×); (c) and (d) Interface between RPC with 3 wt.% of nano-TiO₂ and underside of steel bar (1000×) and (20000×)

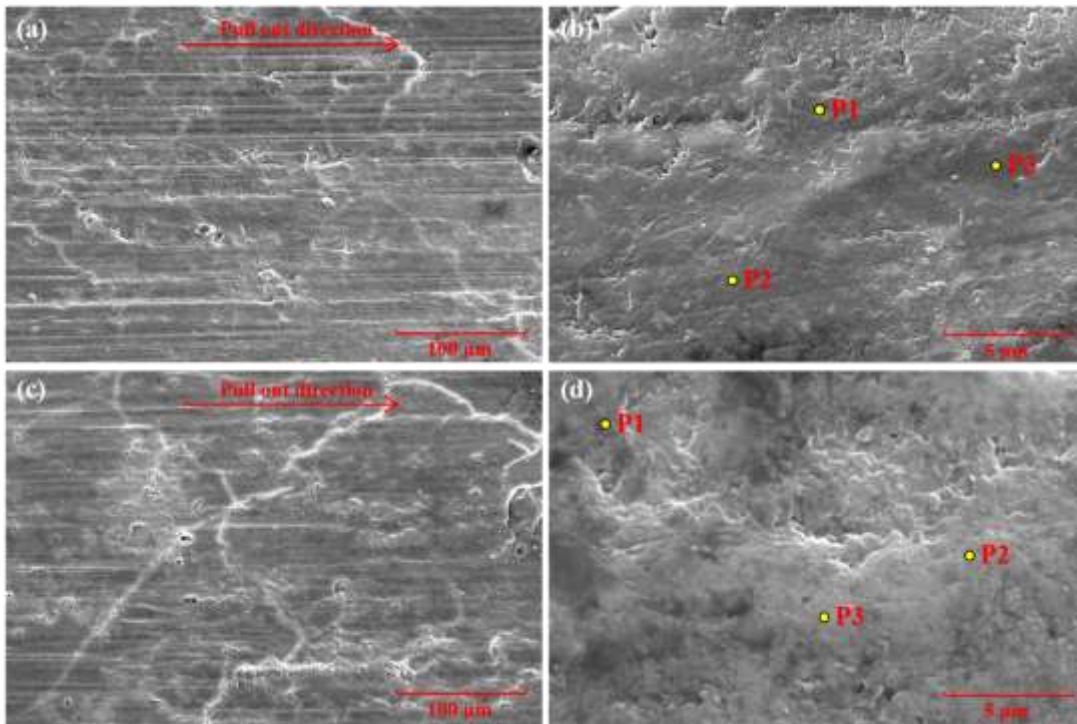


Figure 8. The microstructures of (a) and (b) Interface between RPC with 0.5 wt.% of H-CNTs and upside of steel bar (1000×) and (20000×); (c) and (d) Interface between RPC with 0.5 wt.% of H-CNTs and underside of steel bar (1000×) and (20000×)

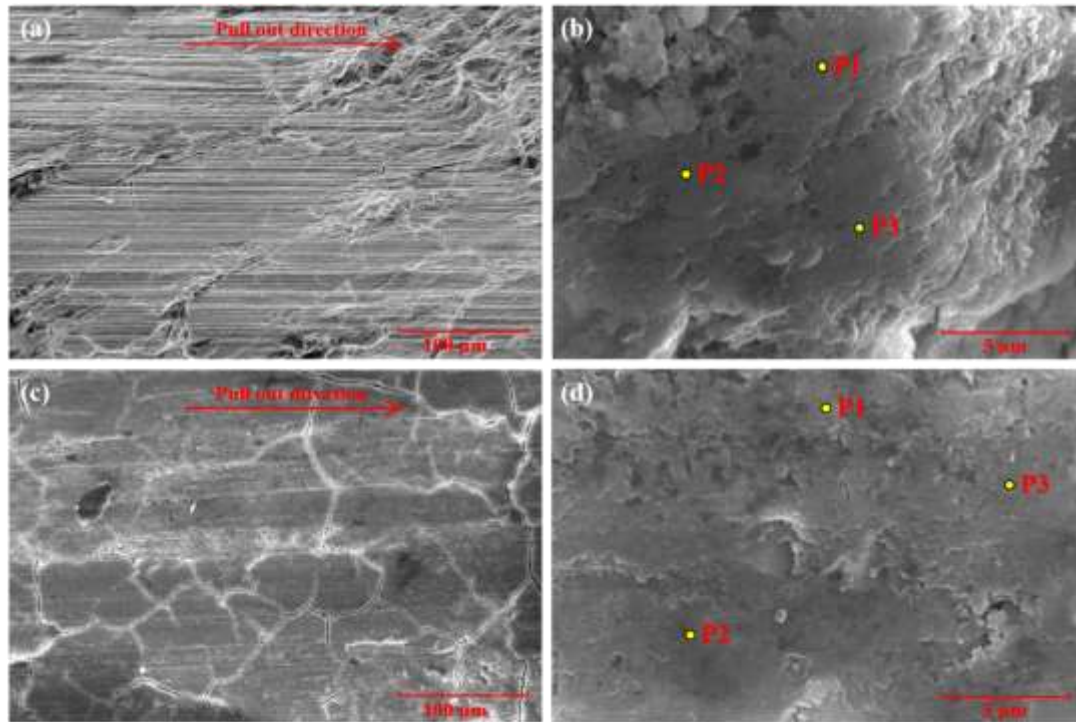


Figure 9. The microstructures of (a) and (b) Interface between RPC with 0.5 wt.% of nano-BN and upside of steel bar (1000×) and (20000×); (c) and (d) Interface between RPC with 0.5 wt.% of nano-BN and underside of steel bar (1000×) and (20000×)

287
288

Table 4. The molar contents of CaO and SiO₂ in the RPC-steel bar interface

Specimen code	Interface between RPC and upside of steel bar				Interface between RPC and underside of steel bar			
	CaO content (%)	SiO ₂ content (%)	Ca/Si ratio	Average Ca/Si ratio	CaO content (%)	SiO ₂ content (%)	Ca/Si ratio	Average Ca/Si ratio
Control	13.30	15.37	0.87	0.86	14.38	13.33	1.08	1.02
	10.53	14.11	0.75		14.80	14.53	1.02	
	17.38	18.31	0.95		18.83	19.32	0.97	
T-3	14.00	16.93	0.83	0.83	22.28	20.44	1.09	1.02
	13.40	16.41	0.82		22.10	23.28	0.95	
	14.27	17.00	0.84		24.16	23.45	1.03	
H-0.1	7.49	13.11	0.57	0.65	11.44	13.49	0.85	0.89
	9.67	14.48	0.67		10.47	12.72	0.82	
	8.63	12.11	0.71		13.18	13.20	1.00	
B-0.5	12.88	16.79	0.77	0.75	14.46	14.37	1.01	0.92
	12.94	19.69	0.66		13.83	14.69	0.94	
	13.74	16.73	0.82		11.97	14.62	0.82	

289
290

The modification of nanofillers on the microstructures of RPC-steel bar interface derives from the nano-core effect, as shown in Figure 10. At the beginning of hydration process, the nanofillers enrich in the RPC-steel bar interface due to the wall effect, as depicted in Figure 5. Owing to the high surface energy, the enriched nanofillers are adhered by C-S-H gels and restrict the generation of CH crystals due to their high

294

295 surface energy [48, 49]. The compact microstructures are conducive to improve the
 296 RPC-steel bar physical bond which is the source of cracking bond strength. Therefore,
 297 the cracking bond strength of RPC-steel bar interface is improved as the nanofillers are
 298 incorporated. Apart from the bond of contact surface, the strength of the interfacial zone
 299 also affects the bond between nanofillers modified RPC and steel bars. For 0-D
 300 nanofillers, the nanofillers act as hard cores wrapped by C-S-H gels, which can deflect
 301 the cracks due to the pinning effect [27]. For 1-D and 2-D nanofillers, the presence of
 302 nanofillers can bridge the adjacent hydration products and notably restrain the
 303 formation of cracks [50, 51]. These effects contribute to the improvement of the
 304 integrity of the RPC-steel bar interfacial zone after cracking, thereby modifying the
 305 ultimate bond strength and residual bond strength of RPC-steel bar interface.
 306

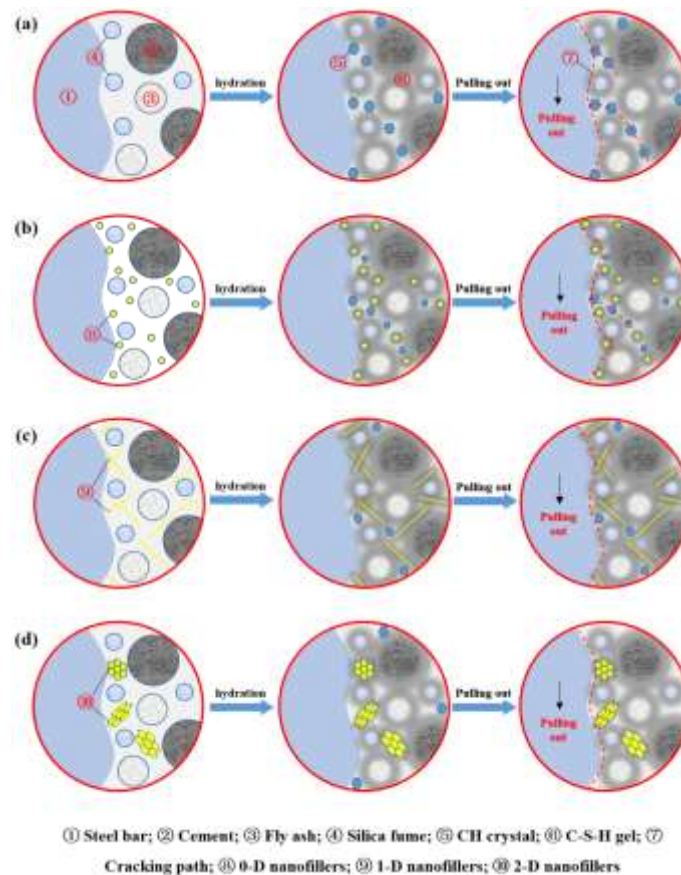


Figure 10. The modifying mechanisms of nanofillers on the RPC-steel bar interface: (a) Specimen without nanofillers; (b) Specimen with 0-D nanofillers; (c) Specimen with 1-D nanofillers; (d) Specimen with 2-D nanofillers

307

308 3.3 Bond stress-slip relationship

309 The bond stress-slip relationship is usually used for describing the bond
310 characteristics between concrete and reinforcing bar. However, the pull-out test can
311 only measure the pull-out load and slip at the loading end and free end. It means the
312 relationship based on the experimental results is only an average constitutive model
313 rather than a real constitutive relationship between concrete and reinforcing bar. When
314 the embedment length of reinforcing bar is short, these two models are approximately
315 equal due to the uniform distribution of bond stress along the reinforcing bar. According
316 to former studies [52, 53], the distribution of bond stress along the steel bar can be
317 regarded as uniform when the embedment length of steel bar equals 5 times the
318 diameter of steel bar. Therefore, the embedment length of steel bar in this study satisfies
319 the hypothesis of short embedment length, that is to say, the average bond stress-slip
320 curve in this study can be used to reflect the bond stress-slip relationship between RPC
321 without/with nanofillers and steel bar.

322 Several models have been proposed to describe the bond stress-slip relationship
323 between concrete and reinforcing bars [38–41, 54]. According to reference [54], the
324 bond stress-slip relationship is modeled as an ascending branch and a constant branch
325 (Figure 11 (a)), given by the following equations:

$$\tau_b = \begin{cases} \tau_b \cdot \left(\frac{s}{s_u}\right)^\alpha & s \leq s_m \\ \beta \cdot \sqrt{f_c} & s > s_m \end{cases} \quad (3)$$

326 where the recommend values of α and s_m are 0.5 and 0.10 mm, respectively, the
327 value of β is suggested as 0.3 and 0.15 for modeling good and bad bond conditions,
328 respectively, and f_c is the cylindrical compressive strength of concrete. However, due
329 to the micro-interlocking and friction between concrete and reinforcing bar, a softening

330 branch generally exists after the bond stress reaches the ultimate bond strength. A model
 331 (called BPE model) considering the softening behavior is, therefore, proposed by
 332 Eligehausen et al. [38]. The BPE model divides the bond stress-slip relationship into
 333 ascending, plateau, descending, and residual branches, expressed by the following
 334 equations:

$$\tau_b = \begin{cases} \tau_b \cdot \left(\frac{s}{s_1}\right)^\alpha & s \leq s_1 \\ \tau_{b,u} & s_1 < s \leq s_2 \\ \tau_{b,u} - p \cdot \frac{\tau_{b,u}}{s_2} \cdot (s - s_2) & s_2 < s \leq s_3 \\ \tau_{b,r} & s > s_3 \end{cases} \quad (4)$$

335 where the α and p are the fitted parameters based on the experiment results, s_1 , s_2 ,
 336 s_3 , and s_4 are the slips at boundaries of different branches, as shown in Figure 11 (b).
 337 In addition, the BPE model was further modified by removing the plateau branch, as
 338 shown in Figure 11 (c), because the softening behavior may immediately take place
 339 when the bond stress exceeds the ultimate bond strength in many experiments [39].
 340 Similarly, different equations, such as the logarithmic equation [40] and polynomial
 341 equation [41], were employed to describe the bond stress-slip relationship containing
 342 the aforementioned three or four branches.

343 However, the concrete strength used in former studies is relatively low, therefore, the
 344 initial branch was not observed and considered in the model. Referring to the previous
 345 models [38–41, 54], a model considering initial, ascending, descending, and residual
 346 branches is proposed, as depicted in Figure 10 (d). First, an initial branch is present
 347 until the slip occurs between RPC and steel bars. Then, the bond-slip curve presents an
 348 ascending branch up to a peak strength value. Next, a descending branch is present until
 349 the bond stress decreases to the residual bond strength. Finally, a horizontal branch,
 350 named residual branch, is present corresponding to a constant value equal to the value
 351 of residual bond strength. The proposed bond-slip model can be expressed as:

$$= \begin{cases} \tau_{b,0} + \frac{\tau_b \arctan(\eta \cdot s/s_u)}{\arctan \eta} (\tau_{b,u} - \tau_{b,0}) & (\\ \tau_{b,u} - \mu \cdot \frac{\tau_{b,u}}{s_u} \cdot (s - s_u) &) \end{cases} \tau_{b,r}$$

352 where η and μ are the fitted parameters based on the experiment results, and other
 353 meanings of parameters refer to section 3.1. Based on least squares fitting criterion,
 354 Figure 12 compares the experimental and analytical stress bond-slip curves of the RPC
 355 without/with nanofillers-steel bar interface and the corresponding analytical fitting
 356 parameters. The goodness of fit (R^2) ranges from 0.9061 to 0.9994, indicating that the
 357 proposed model can well describe the stress bond-slip relationship of RPC without/with
 358 nanofillers and steel bar interface.

359

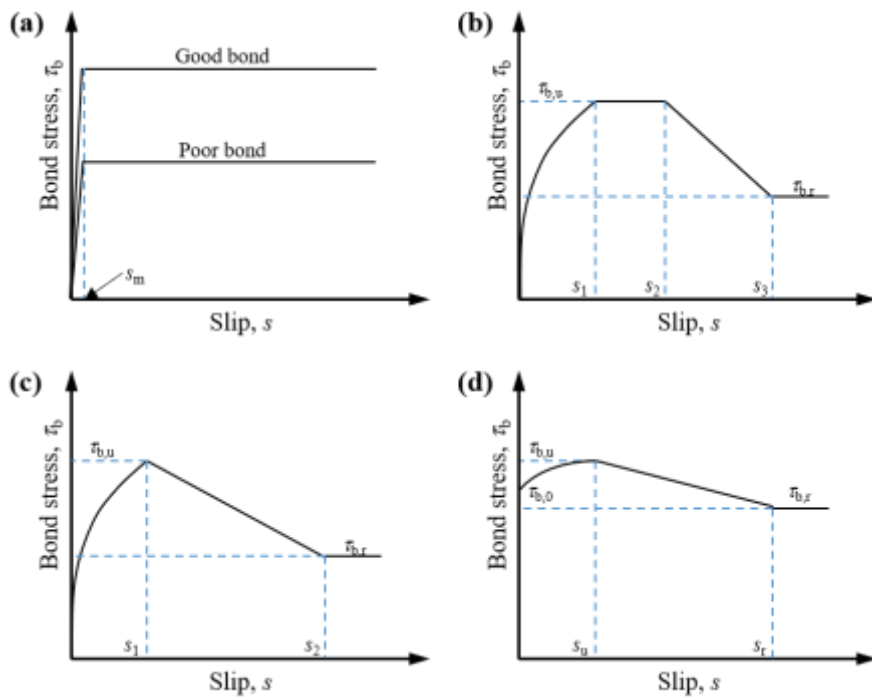
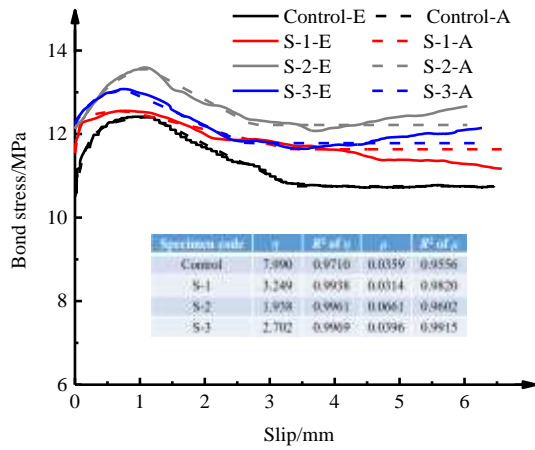
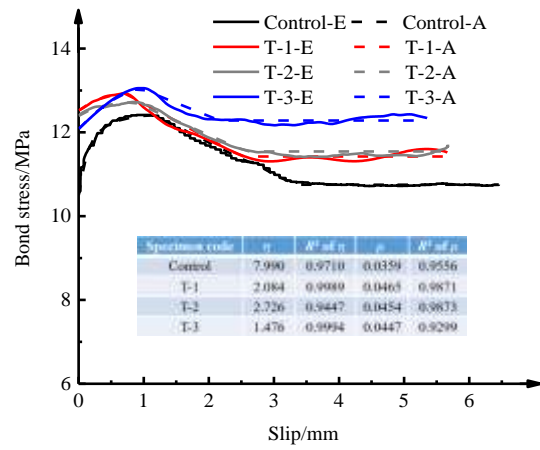


Figure 11. Bond stress-slip model: (a) CEB bond model [54]; (b) BPE model [38]; (c) Modified BPE model [39]; (d) Model proposed in this study

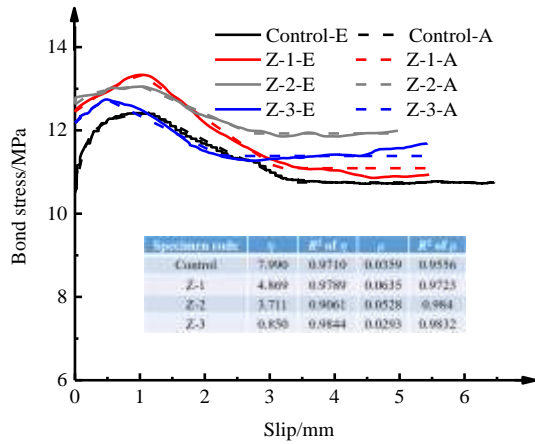
360



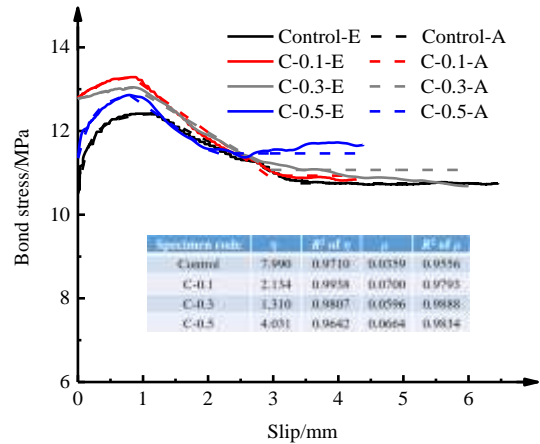
(a) Specimens without/with nano-SiO₂



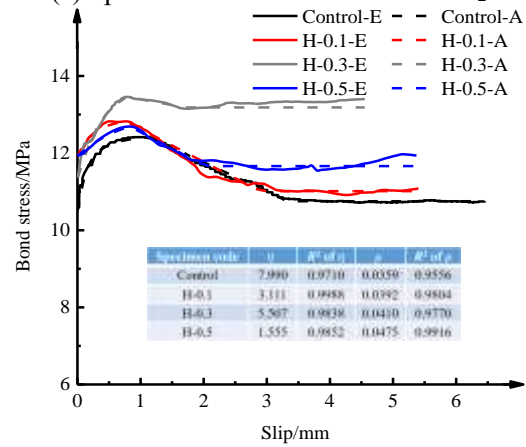
(b) Specimens without/with nano-TiO₂



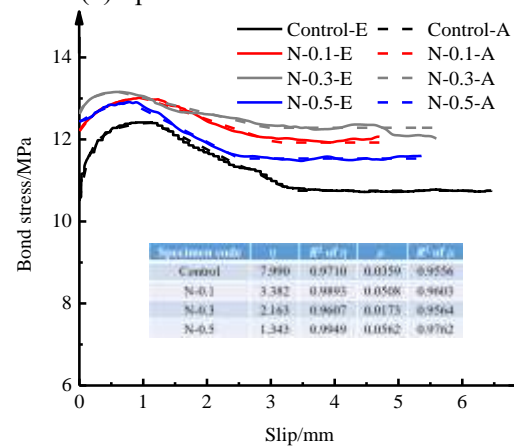
(c) Specimens without/with nano-ZrO₂



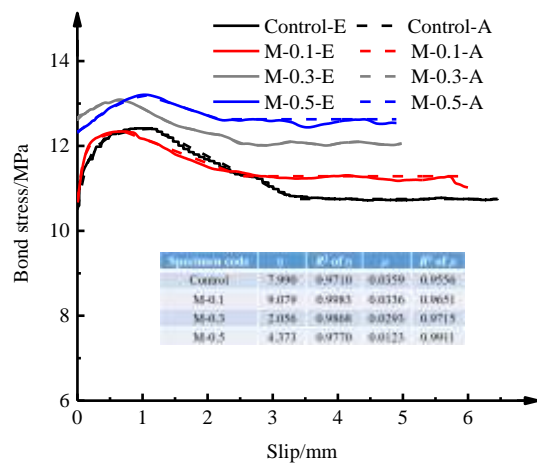
(d) Specimens without/with CNTs



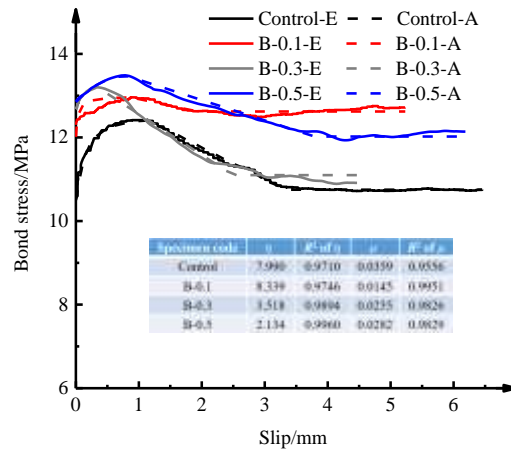
(e) Specimens without/with H-CNTs



(f) Specimens without/with Ni@CNTs



(g) Specimens without/with multi-layer graphene



(h) Specimens without/with nano-BN

Figure 12. Comparison between experimental and analytical bond stress-slip curves (The nomenclature in the legend is specimen code-E/A, which means the experimental (E) results or analytical (A) results of specimen in different group)

361 4 Conclusion

362 The presence of nanofillers increases the bond strength and reduces the slip between
 363 RPC and plain steel bar. The modification of nanofillers depends on their type and
 364 content. The modifying mechanisms of nanofillers on the RPC-steel bar interface can
 365 be attributed to the improvement of the microstructure caused by the nano-core effect
 366 of the nanofillers enriched in the interface. The enriched nanofillers can improve the
 367 compactness of hydration products, reduce the Ca/Si ratio of C-S-H gels in the interface
 368 as well as reduce the defects caused by internal bleeding, enhancing the chemical-
 369 physical adhesion, mechanical micro-interlocking, and friction between nanofillers
 370 modified RPC and steel bars. Owing to these mechanisms, the presence of nanofillers
 371 can significantly improve the microstructure of the interface, especially the underside
 372 near the steel bar, thus modifying the bond behavior between RPC and steel bar. The
 373 proposed model considering initial branch can accurately describe the bond stress-slip
 374 relationship between RPC with/without nanofillers and plain steel bar.

375 The excellent bond stress-slip relationship between RPC with nanofillers and steel
 376 bars, on the one hand, can ensure the stress transfer between RPC and steel bars, as well

377 as hinder the invasion of harmful substances in concrete, preventing steel reinforcement
378 corrosion. This is beneficial for improving the durability of reinforced concrete
379 structures and decreasing the thickness of concrete cover of reinforced concrete
380 structures. On the other hand, it is conducive to improve the ductility of reinforced
381 concrete structure, avoid brittle failure, and gain time for structural monitoring, safety
382 warning, and later repairing. Meanwhile, the revealed mechanisms and the proposed
383 model in this study can provide references for further designing and controlling
384 reinforced concrete elements and structures.

385 Future investigations will focus on the bond behavior between nanofillers modified
386 RPC and ribbed steel bars as well as the performance of full-size reinforced RPC
387 elements modified with nanofillers.

388

389 **Acknowledgements**

390 The authors would like to thank the funding offered by the National Science Foundation
391 of China (51978127 and 51908103), and the Fundamental Research Funds for the
392 Central Universities (DUT21RC(3)039).

393

394 **References**

395 [1] Zhang X, Ou J, Wu Z. Effect of circumferentially nonuniform lateral tension on
396 bond behavior between plain round bars and concrete: Analytical study. *Journal of*
397 *Structural Engineering*, 2017; 143(12): 04017170.

398 [2] Araba AM, Ashour AF. Flexural performance of hybrid GFRP-steel reinforced
399 concrete continuous beams. *Composites Part B-Engineering*, 2018; 154: 321-336.

400 [3] Wang Y, Cai G, Larbi AS, Tsavdaridis KD, Ran J. Monotonic axial compressive
401 behaviour and confinement mechanism of square CFRP-steel tube confined concrete.

402 Engineering Structures, 2020; 217: 110802.

403 [4] Prince MJR, Singh B. Bond strength of deformed steel bars in high-strength
404 recycled aggregate concrete. *Materials & Structures*, 2015; 48(12): 3913-3928.

405 [5] Saleh N, Ashour A, Lam D, Sheehan T. Experimental investigation of bond
406 behaviour of two common GFRP bar types in high-strength concrete. *Construction and
407 Building Materials*, 2018; 201: 610-622.

408 [6] Feldman LR, Bartlett FM. Bond stresses along plain steel reinforcing bars in pullout
409 specimens. *ACI Structural Journal*, 2007; 104(6): 685-692.

410 [7] Mo KH, Alengaram UJ, Jumaat MZ. Bond properties of lightweight concrete-A
411 review. *Construction and Building Materials*, 2016; 112: 478-496.

412 [8] Zhang Z, Jung D, Audrawes B. Evaluation of surface roughness and bond-slip
413 behavior of new textured epoxy-coated reinforcing bars. *Construction and Building
414 Materials*, 2020; 262: 120762.

415 [9] Behnood A, Ziari H. Effects of silica fume addition and water to cement ratio on the
416 properties of high-strength concrete after exposure to high temperatures. *Cement and
417 Concrete Composites*, 2008; 30(2): 106-112.

418 [10] Li LG, Chen ZP, Ouyang Y, Zhu J, Chu SH, Kwan AKH. Synergistic effects of
419 steel fibres and expansive agent on steel bar-concrete bond. *Cement and Concrete
420 Composites*, 2019; 104: 103380.

421 [11] Fehling E, Lorenz P, Leutbecher T. Experimental investigations on anchorage of
422 rebars in UHPC. In: 3rd International Symposium on UHPC and Nanotechnology for
423 High Performance Construction Materials, Kassel, March 7-9, 2012.

424 [12] Wei W, Liu F, Xiong Z, Yang F, Li L, Luo H. Effect of loading rates on bond
425 behaviour between basalt fibre-reinforced polymer bars and concrete. *Construction and
426 Building Materials*, 2020; 231:117138.

- 427 [13] Han B, Dong S, Ou J, Zhang C, Wang Y, Yu X, Ding S. Microstructure related
428 mechanical behaviors of short-cut super-fine stainless wire reinforced reactive powder
429 concrete. *Materials and Design*, 2016; 96: 16-26.
- 430 [14] Wang J, Dong S, Yu X, Han B. Mechanical properties of graphene reinforced
431 reactive powder concrete at different strain rates. *Journal of Materials Science*,
432 2020,55(8):3369-3387.
- 433 [15] Park SH, Kim DJ, Ryu GS, Koh KT. Tensile behavior of ultra high performance
434 hybrid fiber reinforced concrete. *Cement and Concrete Composites*, 2012; 34(2): 172-
435 184.
- 436 [16] Doroud K, Moshaii A, Pezeshkian Y, Rahighi J, Afarideh H. Simulation of
437 temperature dependence of RPC operation. *Nucl Instrum Methods Phys Res Sect A*,
438 2009; 602(3): 723 - 726.
- 439 [17] Lee M, Wang Y, Chiu C. A preliminary study of reactive powder concrete as a new
440 repair material. *Construction and Building Materials*, 2007; 21(1): 182 - 189.
- 441 [18] Alhawat M, Ashour A. Bond strength between corroded steel and recycled
442 aggregate concrete incorporating nano silica. *Construction and Building Materials*,
443 2020; 237: 117441.
- 444 [19] Deng Z, Jumbe RD, Yuan C. Bonding between high strength rebar and reactive
445 powder concrete. *Computers and Concrete*, 2014; 13(3): 489-504.
- 446 [20] Bubshait AA, TahirB. Effect of silica fume on the concrete-steel bond. *Building*
447 *Research and Information*, 1997; 25(6): 365-369.
- 448 [21] Pishro AA, Feng X, Ping Y, Dengshi H, Shirazinejad RS. Comprehensive equation
449 of local bond stress between UHPC and reinforcing steel bars. *Construction and*
450 *Building Materials*, 2020; 262: 119942.
- 451 [22] Dybel P, Furtak K. Influence of silica fume content on bond behaviour of

452 reinforcement in HPSCC. Magazine of Concrete Research, 2018; 70(19): 973-983.

453 [23] Ganeshan M, Venkataraman S, Nirubanchakravarthy L, Sindhu G. Pull out
454 behaviour of deformed steel bars in fly ash blended self compacting geopolymer
455 concrete. Romanian Journal of Materials, 2018; 48(3): 346-354.

456 [24] Noorvand H, Ali AAA, Demirboga R, Farzadnia N, Noorvand H. Incorporation of
457 nano TiO₂ in black rice husk ash mortars. Construction and Building Materials, 2013;
458 47: 1350-1361.

459 [25] Khaloo A, Mobini MH, Hosseini P. Influence of different types of nano-SiO₂
460 particles on properties of high-performance concrete. Construction and Building
461 Materials, 2016; 113: 188-201.

462 [26] Dong S, Wang Y, Ashour A, Han B, Ou J. Nano/micro-structures and mechanical
463 properties of ultra-high performance concrete incorporating graphene with different
464 lateral sizes. Composites Part A-Applied Science and Manufacturing, 2020; 137:
465 106011.

466 [27] Han B, Li Z, Zhang L, Zeng S, Yu X, Han B, Ou J. Reactive powder concrete
467 reinforced with nano SiO₂-coated TiO₂. Construction and Building Materials, 2017; 148:
468 104-112.

469 [28] Han B, Ding S, Wang J, Ou J. Nano-Engineered Cementitious Composites:
470 Principles and Practices. Springer; 2019.

471 [29] Li L, Zheng Q, Han B, Ou J. Fatigue behaviors of graphene reinforcing concrete
472 composites under compression. International Journal of Fatigue. 2021; 151: 106354.

473 [30] Wang X, Dong S, Ashour A, Zhang W, Han B. Effect and mechanisms of
474 nanomaterials on interface between aggregates and cement mortars. Construction and
475 Building Materials, 2019; 240: 117942.

476 [31] Comité Européen de Normalisation, European Standard EN 1998-3. Eurocode 8:

477 Design of structures for earthquake resistance-part 3: Assessment and retrofitting of
478 buildings. Brussels; 2004.

479 [32] Shi X, Xie N, Fortune K, Gong J. Durability of steel reinforced concrete in chloride
480 environments: An overview. *Construction and Building Materials*, 2012; 30: 125-138.

481 [33] Li X, Wu Z, Zheng J, Dong W. Effect of loading rate on the bond behavior of plain
482 round bars in concrete under lateral pressure. *Construction and Building Materials*,
483 2015; 94: 826-836.

484 [34] Dybel P, Furtak K. Influence of silica fume content on the quality of bond
485 conditions in high-performance concrete specimens. *Archives of Civil and Mechanical*
486 *Engineering*, 2017; 17(4): 795-805.

487 [35] Li X, Li M. Multifunctional self-sensing and ductile cementitious materials.
488 *Cement and Concrete Research*, 2019; 123: 105714.

489 [36] Wang X, Dong S, Ashour A, Han B. Bond of nanoinclusions reinforced concrete
490 with old concrete: strength, reinforcing mechanisms and prediction model.
491 *Construction and Building Materials*; 2021;283,122741.

492 [37] Forsyth DA, Ponce J, *Computer Vision A Modern Approach*, New York: Pearson,
493 2012.

494 [38] Eligehausen R, Popov EP, Bertero VV. Local bond stress-slip relationships of
495 deformed bars under generalized excitations. EERC University of California Berkeley.
496 Report No. UCB/EERC 83-23; 1983.

497 [39] Cosenza E, Manfredi G, Realfonzo R. Behavior and modeling of bond of FRP
498 rebars to concrete. *Journal of Composites for Construction*, 1997; 1(2): 40–51.

499 [40] Feldman LR, Bartlett FM. Bond strength variability in pullout specimens with
500 plain reinforcement. *ACI Structural Journal*, 2005; 102(6): 860-867.

501 [41] Xiao J, Falkner H. Bond behaviour between recycled aggregate concrete and steel

502 rebars. *Construction and Building Materials*, 2007; 21(2): 395-401.

503 [42] Chinese National Standard. Specifications for Design of Highway Reinforced
504 Concrete and Prestressed Concrete Bridges and Culverts, JTG 3362-2018. Beijing,
505 2018.

506 [43] Clark LA. *Concrete Bridge Design to BS 5400*. Construction Press, 1983.

507 [44] Stoker MF, Sozen MA. Investigation of prestressed reinforced concrete for
508 highway bridges. Part V: Bond characteristics of prestressing strand. University of
509 Illinois Engineering Experiment Station. College of Engineering. University of Illinois
510 at Urbana-Champaign., 1970.

511 [45] Chu SH, Kwan AKH. A new method for pull out test of reinforcing bars in plain
512 and fibre reinforced concrete. *Engineering Structures*, 2018; 164: 82-91.

513 [46] Scrivener KL, Crumbie AK, Laugesen P. The interfacial transition zone (ITZ)
514 between cement paste and aggregate in concrete. *Interface Science*, 2004; 12(4): 411-
515 421.

516 [47] Maso JC. *Interfacial transition zone in concrete*. Florida: CRC Press; 2014.

517 [48] Han B, Zhang L, Zeng S, Dong S, Yu X, Yang R, Ou J. Nano-core effect in nano-
518 engineered cementitious composites. *Composites Part A-Applied Science and*
519 *Manufacturing*, 2017; 95: 100-109.

520 [49] Wang X, Zheng Q, Dong S, Ashour A, Han B. Interfacial characteristics of nano-
521 engineered concrete composites. *Construction and Building Materials*, 2020; 259:
522 119803.

523 [50] Pang SD, Du H. Enhancement of barrier properties of cement mortar with graphene
524 nanoplatelet. *Cement and Concrete Research*, 2015; 76: 10-19.

525 [51] Sasmal S, Ravivarman N, Sindu BS, Vignesh K. Electrical conductivity and piezo-
526 resistive characteristics of CNT and CNF incorporated cementitious nanocomposites

527 under static and dynamic loading. *Composites Part A-Applied Science and*
528 *Manufacturing*, 2017; 100: 227-243.

529 [52] Verderame GM, Carlo GD, Ricci P, Fabbrocino G. Cyclic bond behaviour of plain
530 bars. Part I: Experimental investigation. *Construction and Building Materials*, 2009;
531 23(12): 3499-3511.

532 [53] Verderame GM, Carlo GD, Ricci P, Fabbrocino G. Cyclic bond behaviour of plain
533 bars. Part II: Analytical investigation. *Construction and Building Materials*, 2009;
534 23(12): 3512-3522.

535 [54] Comite Euro-International du Beton. *CEB-FIP Model Code 1990 (Concrete*
536 *Structures)*. Lausanne, 1993.